New Zealand DEFENCE FORCE
Te Ope Kātua O Aotearoa

DEFENCE TECHNOLOGY AGENCY

Defence Technology Agency

DTA Report 408
NR 1690

DTA Digital Image Correlation Capability

Richard M Stubbing
February 2016

DTA Report 408
NR 1690

DTA DIGITAL IMAGE CORRELATION CAPABILITY

Richard M Stubbing

February 2016

ABSTRACT

Digital Image Correlation (DIC) is a technique for optically acquiring full-field measurements of the displacement and deformation of a surface. This is achieved by observing the surface as it deforms, typically using one or more conventional monochrome digital cameras, and comparing the surface's deformed and undeformed states using optical tracking.

The Defence Technology Agency's Applied Vehicle Systems group has now developed an in-house DIC system. The wide array of variables that determine the measurement precision achievable when using DIC makes it difficult to identify a specific metric quantifying this system's accuracy. However, a conservative estimate is that deformation measurements can be obtained with a precision of 1000 microstrain or better in most cases. Greater precision may be achievable in a number of instances, particularly for cases involving smooth strain fields where significant smoothing can be applied to the measured displacements without detrimentally affecting the results.

This system is now available to enhance the Applied Vehicle Systems group's structural analysis toolset, providing a full-field strain measurement capability for New Zealand Defence Force platforms. In contrast to commercial DIC systems, this in-house system can be fully customised and adapted to suit individual New Zealand Defence Force requirements.

DTA Report 408
ISSN 1175-6594 (Print)
ISSN 2253-4849 (Online)

Published by
Defence Technology Agency
Private Bag 32901
Devonport
Auckland 0744
New Zealand

EXECUTIVE SUMMARY

BACKGROUND

Digital Image Correlation (DIC) is a technique for optically acquiring full-field measurements of the displacement and deformation of a surface. This is achieved by observing the surface as it deforms, typically using one or more conventional monochrome digital cameras, and comparing the surface's deformed and undeformed states using optical tracking.

The strengths of DIC relative to other full-field strain measurement technologies such as various interferometry-based techniques include; modest hardware requirements, ease of scalability and a large range of measurable strains. The only required hardware is one or two digital cameras alongside appropriate lighting. Sample preparation is limited to the application of a speckle pattern to the surface being analysed in cases where it does not already have sufficient visual contrast for tracking.

There are two main categories of DIC: 2D DIC and 3D DIC. 2D DIC utilises only a single camera and is less complex than 3D DIC, both experimentally and computationally, but is limited to applications involving the in-plane deformation of flat surfaces. This limitation exists because out-of-plane displacements cannot be quantified using a single camera and will therefore produce erroneous measurements. 3D DIC removes this limitation by making use of multiple cameras viewing the surface from different perspectives, allowing for features to be located in three-dimensional space through triangulation. This ensures that out-of-plane motion does not cause artificial strains to be reported. The use of 3D DIC does however require that a camera calibration procedure be carried out once the cameras are set up in order to determine their relative position and orientation.

AIM

The Defence Technology Agency set out to develop an in-house DIC capability in order to enhance the Applied Vehicle Systems (AVS) group's structural analysis toolset and to provide a full-field strain measurement capability for New Zealand Defence Force (NZDF) platforms.

RESULTS

The AVS group has now developed an in-house DIC system: Modεm. This system comprises three main components: the DIC software itself, which processes the captured images and allows for the results to be interrogated and visualised; the requisite hardware, such as lighting and cameras; and the image capture software through which the cameras are controlled and camera calibration can be performed. Modεm's primary software component has been developed in MATLAB and is capable of performing both 2D DIC and 3D DIC.

The wide array of variables that determine the measurement precision achievable when using DIC makes it difficult to identify a specific metric quantifying this system's

accuracy. However, a conservative estimate is that deformation measurements can be obtained with a precision of 1000 microstrain or better in most cases. Greater precision may be achievable in a number of instances, particularly for cases involving smooth strain fields where significant smoothing can be applied to the measured displacements without detrimentally affecting the results.

This system is now available to enhance the AVS group's structural analysis toolset, providing a full-field strain measurement capability to NZDF platforms. In contrast to commercial DIC systems, this in-house system can be fully customised and adapted to suit individual NZDF requirements.

The flexibility of DIC as a technique for measuring both displacements and deformations results in a range of potential applications that is very broad. In general however, DIC is typically of the greatest value in applications where full-field results can provide intuitive insight into the behaviour of a structure or component, or where the use of conventional contact-based technologies such as resistance strain gauges is insufficient or overly burdensome.

SPONSOR

SO ASI, DAE

CONTENTS

1. DIGITAL IMAGE CORRELATION

1.1. Overview of the technique

Digital Image Correlation (DIC) is a technique for optically acquiring full-field measurements of the displacement and deformation of a surface. This is achieved by observing the surface as it deforms, typically using one or more conventional monochrome digital cameras, and comparing the surface's deformed and undeformed states.

The displacements of many individual points on the surface, referred to as 'features' or 'tracking subsets', are determined using localised motion tracking. These individual displacement measurements are combined to produce a full-field description of the surface's displacement from which a full-field description of the surface's deformation is then derived. This deformation is expressed in terms of strain and typically reported in either percent or microstrain (με).

Interpolation of the greyscale intensities from the images allows this tracking to be carried out with subpixel accuracy. The nature of this approach however, combined with sources of experimental error such as image noise and imperfect camera optics, means that the greatest measurement precision which is currently claimed to be achievable using DIC is no better than 50 με (0.005%) under ideal conditions.

The strengths of DIC relative to other full-field strain measurement technologies such as various interferometry-based techniques include; modest hardware requirements, ease of scalability and a large range of measurable strains. The only required hardware is one or two digital cameras alongside appropriate lighting. Sample preparation is limited to the application of a speckle pattern to the surface being analysed in cases where it does not already have sufficient visual contrast for tracking. The region being considered can range in size from tens of microns [1] to tens of metres [2] and claimed strain measurement ranges encompass strains of 0.005%-2000% [3].

1.2. 2D vs 3D

If the observations are limited to the in-plane deformation of a planar surface and a camera can be positioned so that its optical axis is normal to that surface then the use of 2D DIC is sufficient and only a single camera is required. If the surface is not flat or if out-of-plane deformation is expected then 3D DIC is required and at least two cameras must be used. This is because the apparent size of an object changes with distance and orientation. If only one camera is used then it is not possible to determine the distance or orientation of a given point to the camera. Out-of-plane motion either towards or away from the camera will therefore be interpreted as biaxial tension or biaxial compression respectively, while out-of-plane rotations may be interpreted as tension or compression depending on whether it causes the surface normal to move closer to or further from the camera.

3D DIC removes this limitation by making use of multiple cameras viewing the surface from different perspectives, allowing for features to be located in three-dimensional space through triangulation. This ensures that out-of-plane motion does not cause artificial strains to be reported. The use of 3D DIC does however require that a camera calibration procedure be carried out once the cameras are set up in order to determine their relative position and orientation. Without this information it would not be possible to triangulate the tracked points.

1.3. Potential applications

Perhaps the most common and obvious application of DIC is to obtain qualitative information about the mechanical performance of a component or structure of interest. The benefit of having access to full-field rather than point-wise strain measurements is often significant, particularly for cases where the geometry is complex or the load case poorly understood. In these cases, having access to full-field strain measurements allows the investigator to develop a more comprehensive understanding of the load paths through the component and of the location and severity of stress concentrations. Even for cases where the stress distributions are thought to be relatively well understood, full-field measurements may prove useful by revealing unexpected features of the component's response.

Interesting mechanical behaviour was revealed, for example, when DIC was used to observe the deformation of polyurethane/steel sandwich composite specimens as part of an investigation performed by the Defence Technology Agency (DTA) on behalf of the Royal New Zealand Navy. The purpose of this investigation was to determine the mechanical performance of such structures at a range of temperatures [4]. The DIC results showed that the strain distribution in the cores was highly dependent on temperature, which has implications for the maximum deflection that the structure can sustain before the core is permanently deformed. This fact was not apparent in the conventional experimental measurements.

When trying to obtain material performance data, the use of DIC can be coupled with finite element modelling in order to experimentally determine the material's mechanical properties. An advantage of using full-field data to obtain constitutive properties is that experiments do not need to be optimised to maximise the importance of a single parameter – multiple parameters can instead be determined from a single experiment involving a complex load state. One technique for achieving this is Finite Element Model Updating (FEMU) [5], where a subroutine runs successive finite element simulations in order to determine the material parameters that minimise the difference between the computed deformation and the experimental data. Conversely, this approach can also be used to quantify applied loads if they are not well understood but the material properties are. Often the purpose of carrying out these experiments is to validate the performance of numerical models and enhance their utility as a design tool. This is because validation of numerical models using full-field measurements is significantly more robust than relying on measurements of point-wise behaviour and therefore provides greater confidence in the model's predictions.

DIC can also be a useful tool for analysing events with very short durations, although the nature of the required high speed cameras necessarily means that the achievable spatial resolution and measurement precision are significantly lower than is achievable under more typical conditions. This is particularly true for cases where multiple cameras are utilised to obtain three-dimensional displacement measurements. When utilising high speed cameras the obtained strain fields are typically of relatively poor quality, with the displacement results often being the primary focus instead. As with other applications, the greatest value of these results is often that they can be used to verify the accuracy of numerical simulations in order to enable further analysis.

An example of this is the use of high speed 3D DIC to analyse the response of laminated glass to blast loading [6]. The full-field results were compared to the predictions produced by a finite element model, as shown in Figure 1, in order to determine its potential utility as a design tool. The performance of high speed DIC when analysing synergistic blast and projectile events outside of a laboratory environment was also assessed by the Australian Defence Force's Defence Science and Technology Organisation with promising results [7].

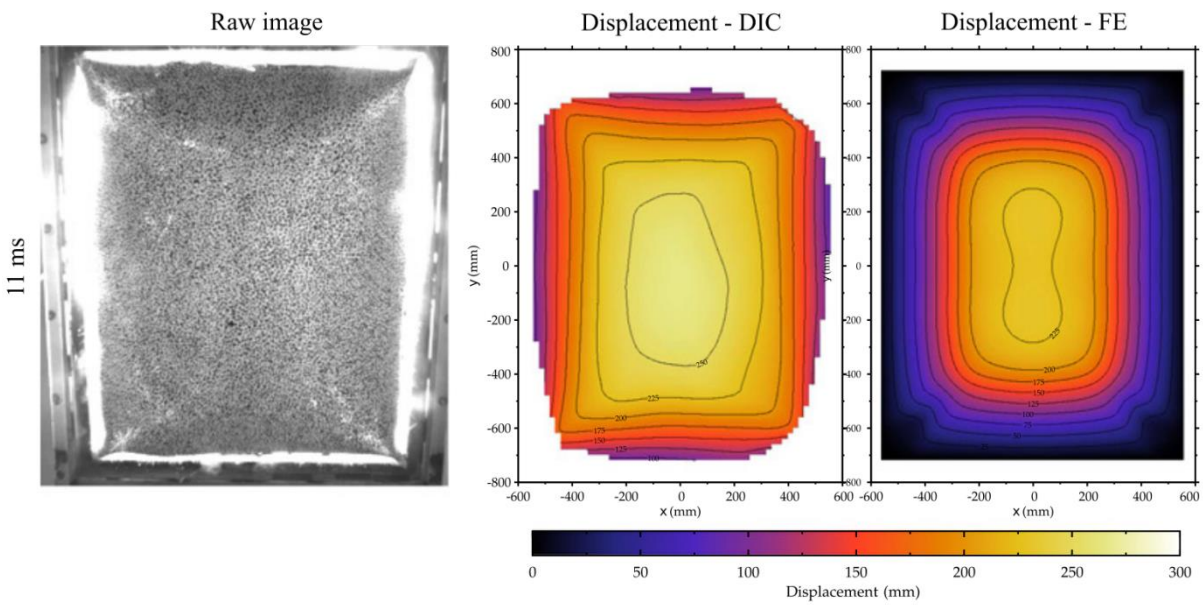

Figure 1: Measured vs. predicted out-of-pane displacement of a glass panel subjected to blast loading [6]

While a focus on the displacement results in high-speed applications is often out of necessity, there are of course instances where the acquisition of displacement measurements is the primary motivation for employing DIC. Examples of this include the measurement of crack opening, or of the compliance of a component or joint.

One such application that was previously investigated by DTA was non-destructive testing of the UH-1H main rotor grip pad, which was prone to delaminating from the blade root. The accepted technique for detecting delamination of the grip pad required that the blades be removed from the airframe in order for the inspection to be performed. DIC, however, presented the possibility for in-situ inspections to take

place through measurement of bond line compliance as the blade tips were deflected, significantly reducing the associated maintenance burden. While the results of this investigation were promising it was concluded that a 3D DIC capability was required, which was not available at the time.

Another proposed DIC application focussed on the measurement of displacements is assessment of the vibrational behaviour of large dynamic structures such as rotorcraft blades. The literature includes a proof of concept demonstration where vinyl targets were applied to the upper surfaces of a pair of Robinson R44 main rotor blades, as shown in Figure 2, and their position in space tracked using high speed 3D DIC during both a ground run and a hover test [8]. Analyses of the blades' vibration modes were then produced using these measurements.

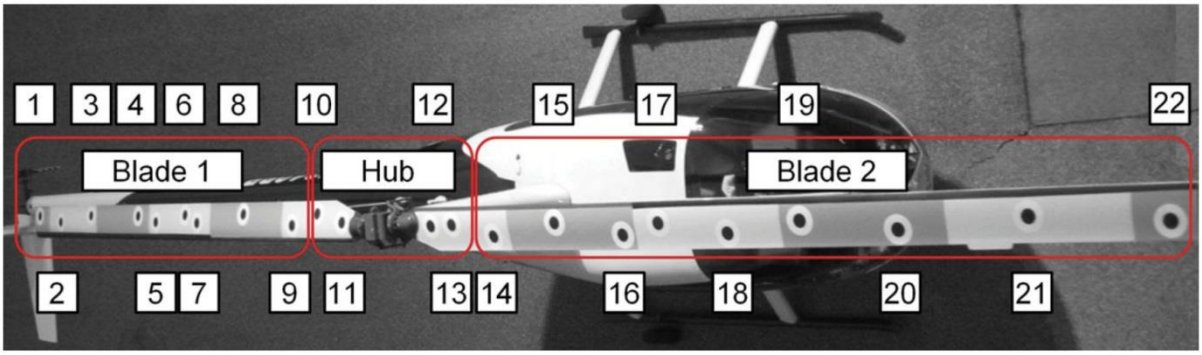

Figure 2: Vinyl targets applied to the upper surfaces of a pair of Robinson R44 main rotor blades [8]

The flexibility of DIC as a technique for measuring both displacements and deformations results in a range of potential applications that is very broad; presenting an exhaustive list here is therefore impractical, although some specific examples are examined in section 3.1. In general however, DIC is typically of the greatest value in applications where full-field results can provide intuitive insight into the behaviour of a structure or component, or where the use of conventional contact-based measurement techniques proves to be burdensome.

2. THE AVS DIC SYSTEM: MODEM

2.1. Overview

The Applied Vehicle Systems (AVS) group has recently developed an in-house DIC system: Modεm (**M**ATLAB **o**ptical **d**isplacement and **strain m**easurement). This system comprises three main components: the DIC software itself, which processes the captured images and allows for the results to be interrogated and visualised; the requisite hardware, such as lighting and cameras; and the image capture software through which the cameras are controlled and camera calibration can be performed. The hardware currently utilised by Modεm is illustrated in Figure 3.

Figure 3: Hardware for the Modεm DIC system

Modεm's primary software component has been developed in MATLAB and is capable of performing both 2D DIC and 3D DIC. As it has not been compiled, the software requires MATLAB to be installed on the host machine in order to be run. This limitation could however be overcome if necessary using the 'MATLAB Compiler' toolbox. Details regarding the code's structure and the utilised techniques are given in section 2.2.

In order to acquire high quality images the surface of interest must be well lit. This is currently achieved through the use of LED panels in combination with linear polarising filters. LED lighting is generally utilised for DIC as the general confinement of their emitted energy to the visible spectrum minimises the introduction of thermal strains. The use of polarising filters with both the lights and the cameras allows for specular reflections to be blocked; these are undesirable as they can cause the local appearance of the surface to change significantly depending on its orientation, leading to the acquisition of poor or invalid tracking results.

The cameras used are a pair of iDS UI-2280SE-M-GL USB cameras incorporating 5 megapixel Sony ICX655 monochrome sensors. For DIC the most important performance characteristics of a camera are typically image noise and sensor resolution. Monochrome sensors are also strongly recommended, as typical colour cameras rely on interpolation to obtain red, green and blue intensity values at each pixel. The imperfect nature of this interpolation introduces small errors into the images which subsequently introduce errors into the reported strain fields [9]. Custom software was written in Python for controlling the cameras and performing both mono and stereo calibration. This software is discussed in detail in section 2.3.

2.2. Modεm code details

The basic structure of the Modεm software is illustrated in Figure 4. The following sections describe the aspects of the software that are of technical interest; more general information regarding user workflow is outside the scope of this report.

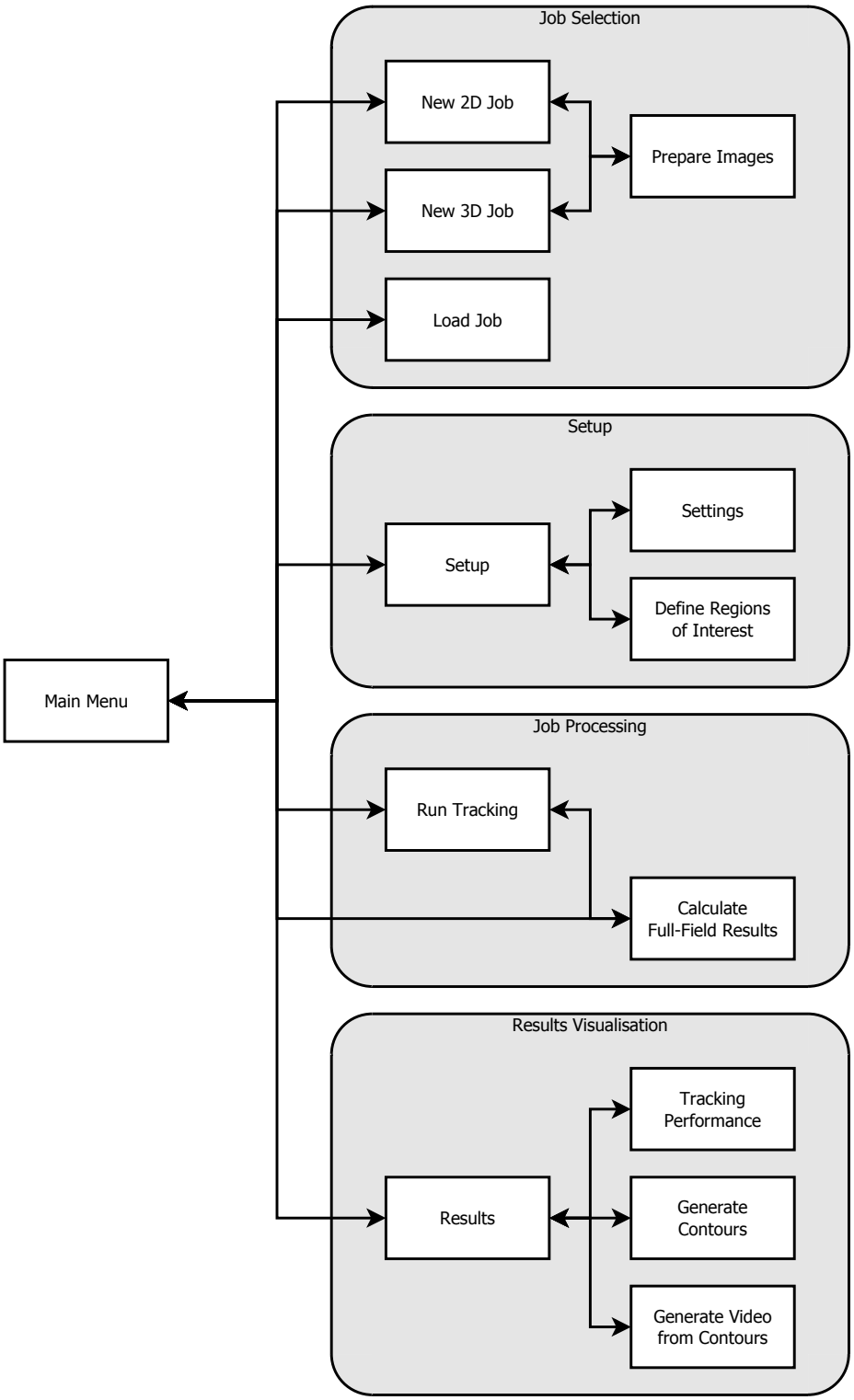

Figure 4: Basic structure of Modεm's primary software component

2.2.1. TRACKING

Before feature tracking is performed, local regions are identified in the image which contain the greatest contrast and are therefore the most likely to provide an accurate tracking result. This first involves assigning a quality value to each pixel coordinate by using Shi-Tomasi corner detection [10]. The coordinates corresponding to the local quality maxima which exceed a smoothed description of these same values by a user defined scaling factor are then selected to be tracked. Adjustment of the parameters of the applied smoothing allows the user to strike a balance between rejection of poor quality features in small low contrast regions, which are not needed due to their proximity to better tracking candidates, and retention of the best features in large low contrast regions.

By default, the initial feature coordinates are then each shifted by a random subpixel value. This reduces the severity of artefacts that can be visible in the full field results due to imperfect intensity interpolation, as the associated tracking errors destructively interfere during regularisation of the raw tracking results [11].

Tracking in Modεm is performed using a pyramidal implementation [12] of the inverse compositional Gauss-Newton tracking algorithm [13], and optionally makes use of a rigid, affine, irregular or quadratic shape function (also known as a warp). In the case of a rigid shape function, the appearance of the tracking subset under consideration is assumed to remain unchanged between the current frame and the reference frame. The algorithm may however fail to converge on a tracking solution or produce a poor result if the subset's appearance has in fact changed appreciably between the two frames. Use of the affine, irregular or quadratic shape functions makes the tracking more robust by solving for additional parameters that describe the subset's deformation between the two frames, but the algorithm's computational cost is consequently increased.

The method utilised for intensity interpolation is user selectable, although the options available are dependent on the selected shape function. If a non-rigid shape function is selected, interpolation is performed using MATLAB's 'griddedInterpolant' and the available interpolation methods are restricted to linear and cubic B-spline. If a rigid shape function is selected, the available interpolation methods also include a range of cubic polynomial interpolants. In this case, all of the methods other than cubic B-spline make use of matrix convolution to perform the interpolation. This form of interpolation is very computationally efficient, but is incompatible with the use of a non-rigid shape function. The cubic interpolation kernels were produced using the interpolant optimisation approach described in section 5.6.1.2 of [14]. While the larger interpolation kernels produce objectively better results, in most cases the benefit of having more than 6 pixels of support is negligible. The use of the 6-tap cubic interpolation method is therefore recommended for general use when a rigid shape function has been selected, otherwise the cubic B-spline method should be used. The use of linear interpolation is not recommended.

For each frame, tracking is reattempted if more than 2 percent of the currently active features are not successfully tracked. The tracking results for those features which were successfully tracked are first used to produce estimates of the displacements and warps across the region of interest. These estimates are then used as initial

guesses for the tracking solutions of each of the features which were lost. Tracking attempts are performed iteratively in this manner until the recovery success rate of the latest iteration is less than 10 percent. It should be noted that other approaches exist that are likely to be more computationally efficient, and could provide an opportunity for future improvement of the software. One such approach is described in [15].

If lens distortion coefficients are available, the reported tracking coordinates are modified according to the iterative distortion correction procedure described in [16]. These coefficients will typically be available when performing 3D DIC, as they are usually determined at the same time as the relative position of the two cameras is determined. For 2D DIC a camera calibration procedure must be performed specifically for this purpose. The use of low distortion optics may mean that this procedure is not required, as the impact on the results is often relatively minimal. If using a camera with moderate or high distortion optics however, the use of distortion calibration and correction is strongly recommended.

2.2.2. STEREO CORRELATION

In Modεm, stereo correlation is achieved by performing an initial correlation between the first frames of each of the two image streams and then processing each of the image streams as independent jobs. This minimises the number of times that correlation must be performed between the image streams, which is desirable as this correlation is relatively computationally expensive [17]. The initial correlation is performed using the same algorithms that are employed for intra-sequence tracking, but using independently selected tracking parameters. Specifically: tracking must be performed using a quadratic shape function to allow for the perspective distortion that takes place between the two cameras; and a large pyramidal height is typically selected to allow for the large apparent displacement that may occur between the two views.

Once coordinates are available for each feature in each of the two image streams, stereo triangulation is performed using the optimal triangulation method described in [18]. This procedure returns the 3D coordinates of each of the features for each image pair, measured in relation to the position of the primary camera.

2.2.3. STRAIN CALCULATION

Prior to calculation of the strain fields, the displacement results must first be smoothed. This is because the displacement results are typically too noisy for the direct derivation of strain results from the raw data to yield desirable results [19]. In Modεm this smoothing is achieved using a penalised regression function that is similar to a thin-plate smoothing spline. This smoothed description of the displacement measurements is evaluated at a set of points that (from the perspective of the primary camera) forms a uniformly spaced rectangular grid when the surface of interest is in its undeformed state; this simplifies the strain calculation procedure by allowing the first order partial derivatives of displacement to be obtained using a simple gradient function.

Due to the way that these partial derivatives are assessed, care should be taken when interpreting the strain results in cases where the optical axis of the primary camera is not normal to the surface in its undeformed state. This is because the surface's deformation is measured relative to a point's local coordinate system, for which the x and y directions are determined by the location of neighbouring points in the results grid; i.e., a line drawn from the left neighbour to the right neighbour points in the x direction, and a line drawn from bottom neighbour to the top neighbour points in the y direction. As mentioned previously, the nodes at which the surface's deformation is assessed form a uniformly spaced rectangular grid from the perspective of the primary camera. This means that analysis of a surface that is viewed at an angle by the primary camera may yield a results grid that, when the surface is viewed straight-on, appears distorted. This is illustrated in Figure 5, where a curved surface is shown both from the perspective of the primary camera (left) and from a relatively straight-on perspective (right). A consequence of this is that the x and y directions, as well as the reported strains, may not have the expected orientation. The results should be interpreted with this in mind.

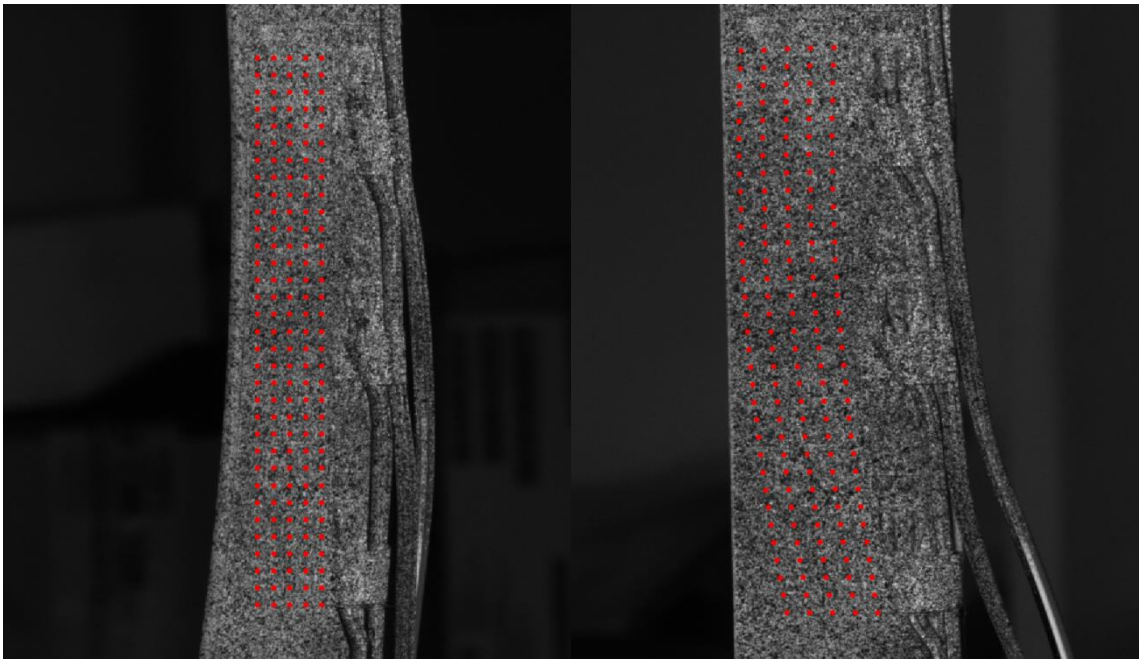

Figure 5: Distortion of the results grid when the optical axis of the primary camera is not initially normal to the surface of interest

Once the partial derivatives of displacement have been obtained for each node of the results grid they are used to generate the right Cauchy-Green deformation tensor for each point. For 2D DIC there are only four partial derivatives that are non-zero, all of which are obtained directly from the displacement field. For 3D DIC however there are nine partial derivatives to consider, only six of which can be directly obtained; the partial derivatives with respect to the z direction are not available because by definition the surface under consideration lies on the local coordinate system's xy-plane. Enforcing a plane-strain condition however produces a system of equations that can be solved to obtain the remaining three, as demonstrated in Appendix A.

An additional complication with 3D analyses is that the inclusion of depth information produces results grids that are not uniformly spaced in their initial state. Although this initial deformation of the grid is associated with a reported initial strain state that is non-zero, these artificial strains are simply subtracted from the results.

2.3. Capture software details

A program called “uEye Sequence Capture” has been developed at DTA to facilitate the capturing of images using AVS group’s iDS uEye cameras for the purpose of DIC. Details regarding the use of this software are available in [20]. uEye Sequence Capture has been written in the Python programming language and makes use of a custom Cython [21] wrapper for the uEye driver’s C API in order to control the uEye cameras. The program has been packaged as a portable executable file using Python’s PyInstaller module.

The software provides the ability to both capture image sequences during experiments and perform a camera calibration. In both cases this can be done either for a single camera or for a pair of cameras. Camera calibration is performed using the calibration functions provided in OpenCV [22].

OpenCV’s camera calibration functions are capable of solving for a range of optical distortion parameters, including radial distortion coefficients up to the 6th order and tangential distortion coefficients. It is however possible to set any number of the parameters to zero when the functions are called, which provides flexibility regarding the optical distortion model that is used to describe the combined characteristics of the chosen cameras and lenses. An investigation into the interaction between the utilised distortion model and the reported strain results revealed that, for the hardware currently utilised by Modεm, the use of a second order symmetric radial distortion model is the most appropriate. With only one non-zero parameter out of the five potential distortion coefficients, this distortion model is particularly simple. It was however found to satisfactorily describe the distortion characteristics of the utilised hardware. The advantage of using a simple model is that it reduces the likelihood of producing a poor calibration, particularly when using relatively few calibration images.

3. PERFORMANCE OF MODEM

3.1. Example applications

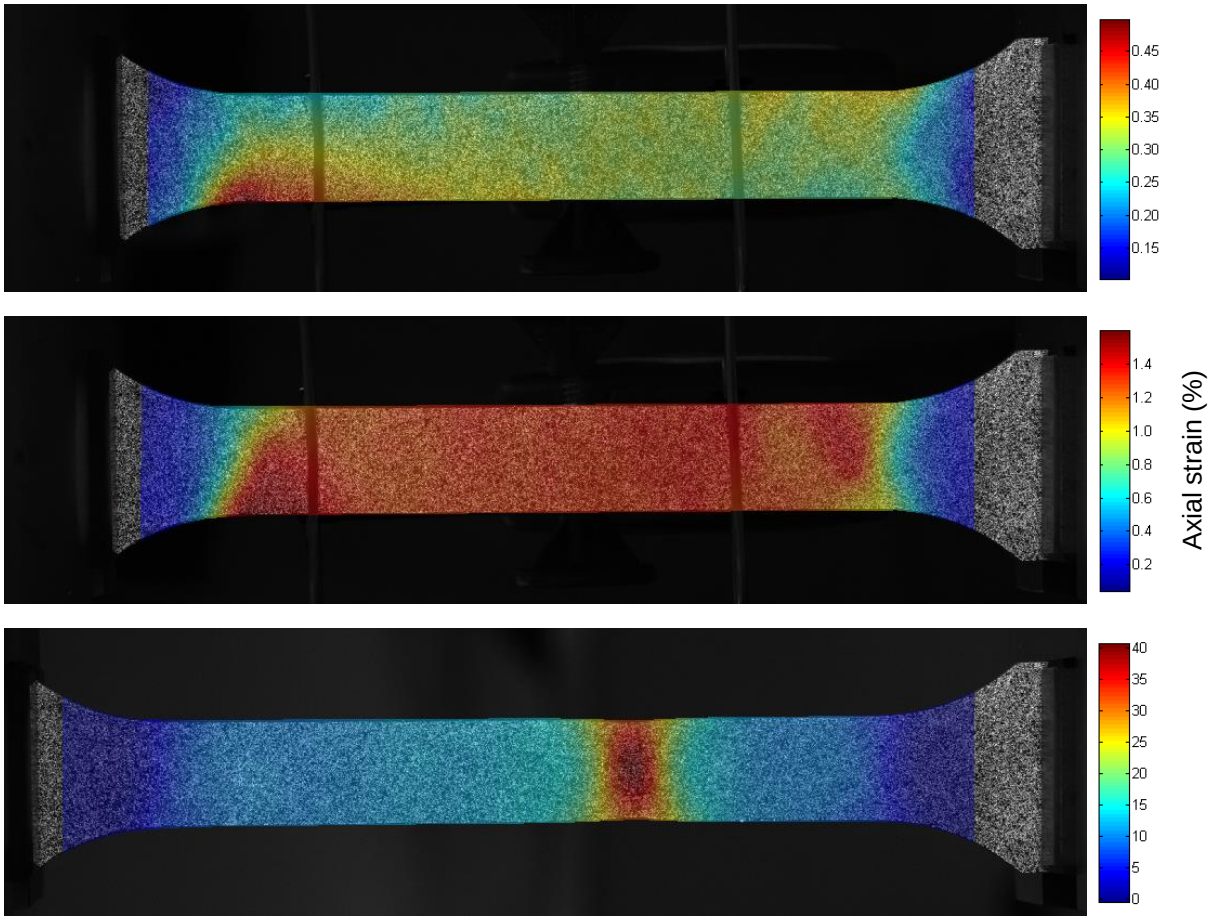

Figure 6: Strain distribution in an aluminium tensile specimen during the elastic (top), plastic (middle) and necking (bottom) phases of the response [Note: the dark vertical lines visible in the upper two images are extensometer clips]

The axial strains measured in an aluminium tensile specimen at various stages of a tensile experiment are illustrated in Figure 6. The three images, from top to bottom, are representative of the specimen's deformation during the elastic phase of the test, during the plastic phase of the test, and shortly prior to failure.

2D DIC is well suited to this type of application, as it involves a flat surface and the presence of out-of-plane displacements and rotations is minor. The use of 3D DIC would typically only be required for tests of this nature when a particularly high degree of accuracy is desired.

In this particular case the availability of full-field strain measurements makes it clear that the specimen is imperfectly aligned in the test fixtures, as evidenced by the asymmetry of the strain field in the uppermost image. This observation serves to highlight the value of full-field measurements, as this issue would be difficult to

identify using only extensometers and strain gauges. The experiment also serves to illustrate the large range of strains which DIC can be used to measure, with the system comfortably measuring strains ranging from 0.1% to 50% and higher over the course of the test.

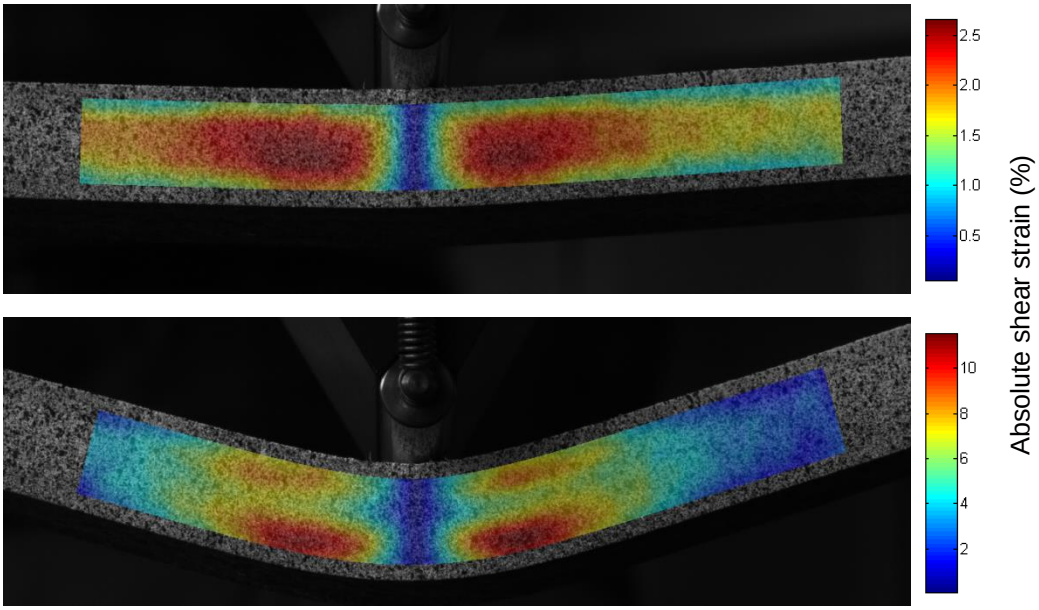

Figure 7: Strain distribution in a polyurethane/steel sandwich composite specimen subjected to three-point bending at approximately 20°C

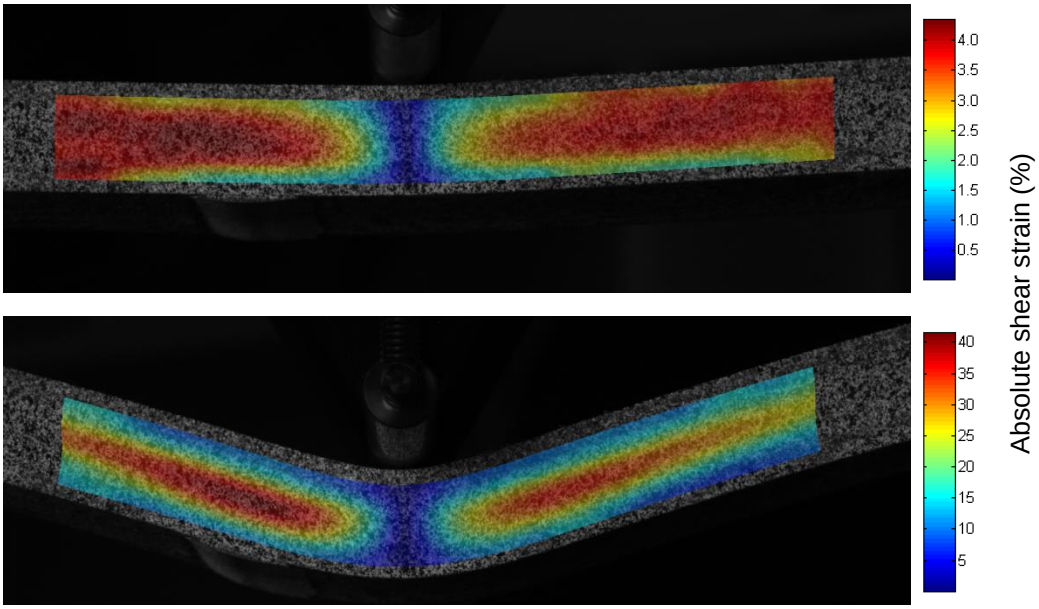

Figure 8: Strain distribution in a polyurethane/steel sandwich composite specimen subjected to three-point bending at approximately 50°C

The absolute shear strains measured in the cores of two polyurethane/steel sandwich composite specimens subjected to three-point bending are illustrated in Figure 7 and Figure 8 (note the different contour scales). The specimen in Figure 7

was at the ambient temperature during the test, which the specimen in Figure 8 was preheated to 50°C.

Although these experiments involved flat surfaces and in-plane loads, the use of 3D DIC was actually desirable in this case. The first reason for this was that the polyurethane cores were sufficiently compliant that they exhibit significant out-of-plane deformation, bulging outwards as the specimens were subjected to loading. The second reason was that the primary camera was not able to be positioned so that its optical axis was normal to the observed surface, but was instead positioned so that it was looking up at the specimen in order to ensure that the loading pin did not obstruct the camera's view of the surface as the specimen deflected downwards. The distance between the camera and much of the specimen therefore decreased over the course of the experiment, which lead to the introduction of a positive strain error into the measurements. The large magnitude of the strains exhibited by the cores during the experiments does however mean that this error may be tolerable depending on how the results are to be utilised. The severity of the strain errors is discussed in section 3.2.

Also of note was that the large deflections involved can limit the achievable spatial resolution. This is because the cameras must be positioned in such a way that the field of view includes the full range of locations that the surface will sweep through over the course of the experiment.

The failure mode was found to change between the heated and the unheated experiments, with the preheated specimens exhibiting fractures along the centreline of the cores, parallel to the skins, and the unheated specimens instead fracturing in the vicinity of the lower skins. The availability of full-field strain measurements revealed that specimens behaved differently even very early in the experiments, with strain localisations evident in the locations that would eventually fracture at an early stage. The full-field measurements also revealed that the cause in this change of behaviour was the transition from bending dominated deflection to shear dominated deflection when the specimens were heated, with the preheated specimens exhibiting significantly higher shear strains in the core for any given deflection.

Figure 9 shows the maximum principal strain measured in a curved carbon fibre reinforced plastic beam subjected to four-point bending during an interlaminar tensile test. In contrast to the previous examples, the primary purpose of this experiment was not to measure the strains in the specimen, but to identify the onset of fracture before it was readily visible. The strain measurements reported by Modεm are derived based on the assumption that the strain distribution within the region of interest is continuous. Fractures, being a discontinuity, therefore appear in the results as a significant strain localisation. In this experiment a very low level of smoothing was employed. This of course yields results which are relatively noisy, but makes the presence of any fractures in the specimen more apparent.

The images illustrate the strain distribution measured in the specimen: at one third of the deflection at which fracture was observed (top), at two thirds of the deflection at which fracture was observed (middle), and immediately after fracture was observed (bottom). The DIC measurements revealed that significant strain localisation, and

possibly fracture, occurred at only one third of the deflection that was required to produce an obvious failure.

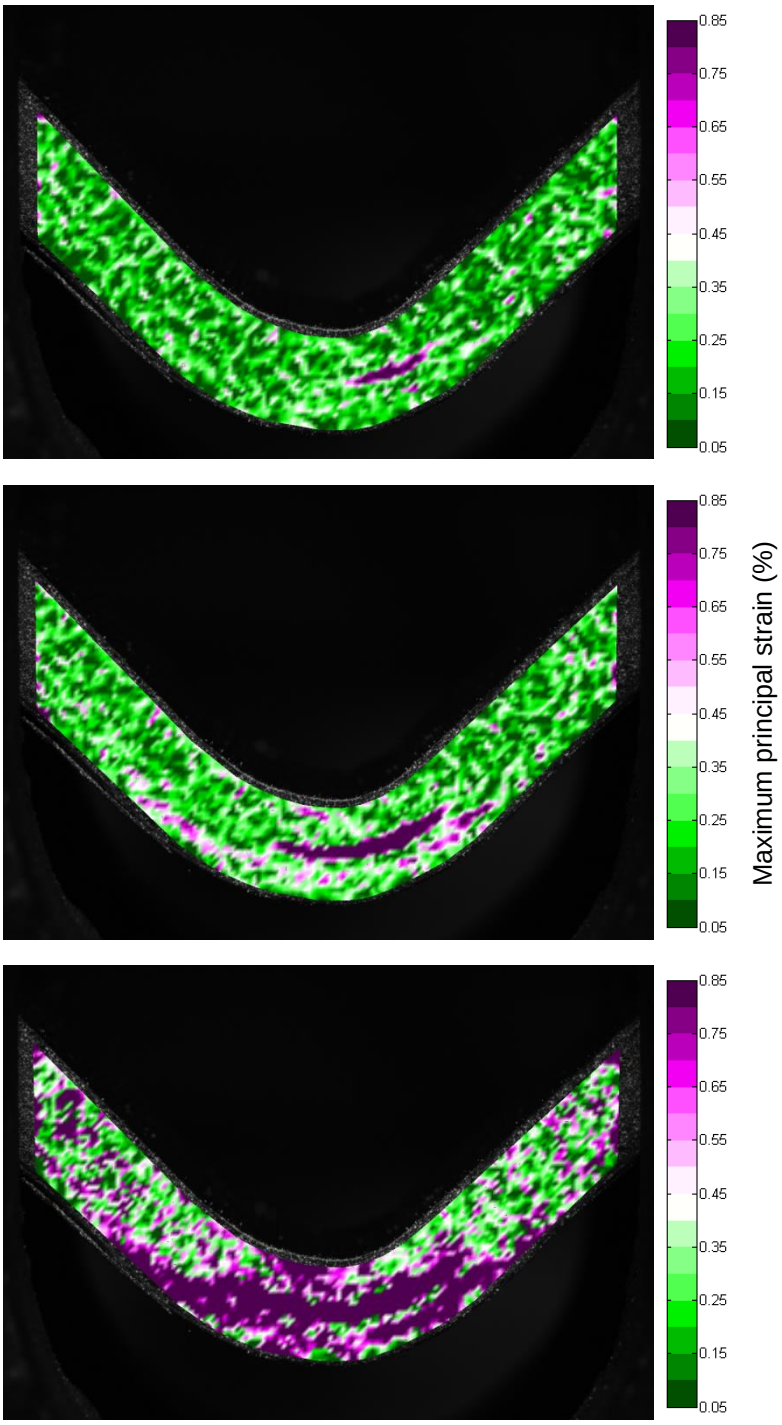

Figure 9: Strain distribution in a curved carbon fibre reinforced plastic beam subjected to four-point bending during an interlaminar tensile test

3.2. 2D vs 3D performance

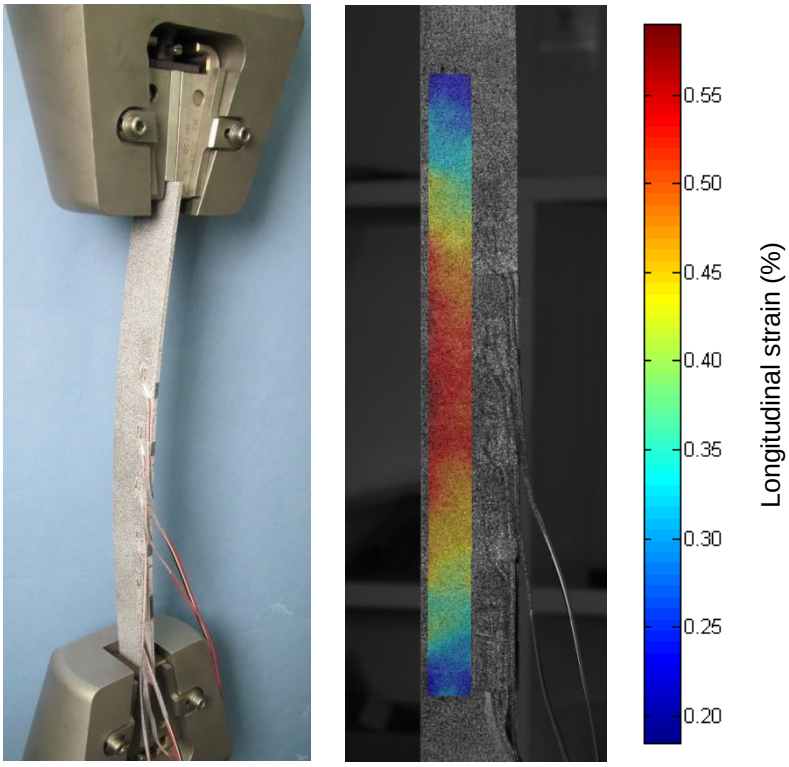

Figure 10: Experimental setup (left) and longitudinal strain measured using 3D DIC (right) in a simply supported thin PVC specimen loaded in compression

As mentioned previously, out-of-plane displacements, non-planar surfaces and viewing angles can all cause errors in the reported strain measurements when using 2D DIC. The use of 2D DIC will, for example, report erroneous strain measurements when used to analyse experiments involving buckling. One such experiment is illustrated in Figure 10.

In order to illustrate the potential impact of selecting 2D DIC for the analysis of experiments of this type, Figure 11 provides a comparison of the strain results generated using both 2D and 3D DIC against strain gauge measurements taken along the length of the specimen. (It should be noted however that this comparison is not perfect; PVC is compliant enough for strain gauges to appreciably reinforce the specimen, resulting in slightly under-reported strains [23].)

It can be seen in Figure 11 that there was a very good correlation between the strain gauge readings and the full field strains reported using 3D DIC. The use of 2D DIC, however, produced results for which the real component of the strain readings was dwarfed by the errors that resulted from the out-of-plane displacements and rotations. The strains reported close to the middle of the specimen can be seen to have large positive errors due to the out-of-plane displacement, which caused apparent tensile strains as the distance between the camera and the specimen decreased. Conversely, the strains close to the ends of the specimen had large

negative errors, as out-of-plane rotation in this case caused apparent compressive strains in the longitudinal direction.

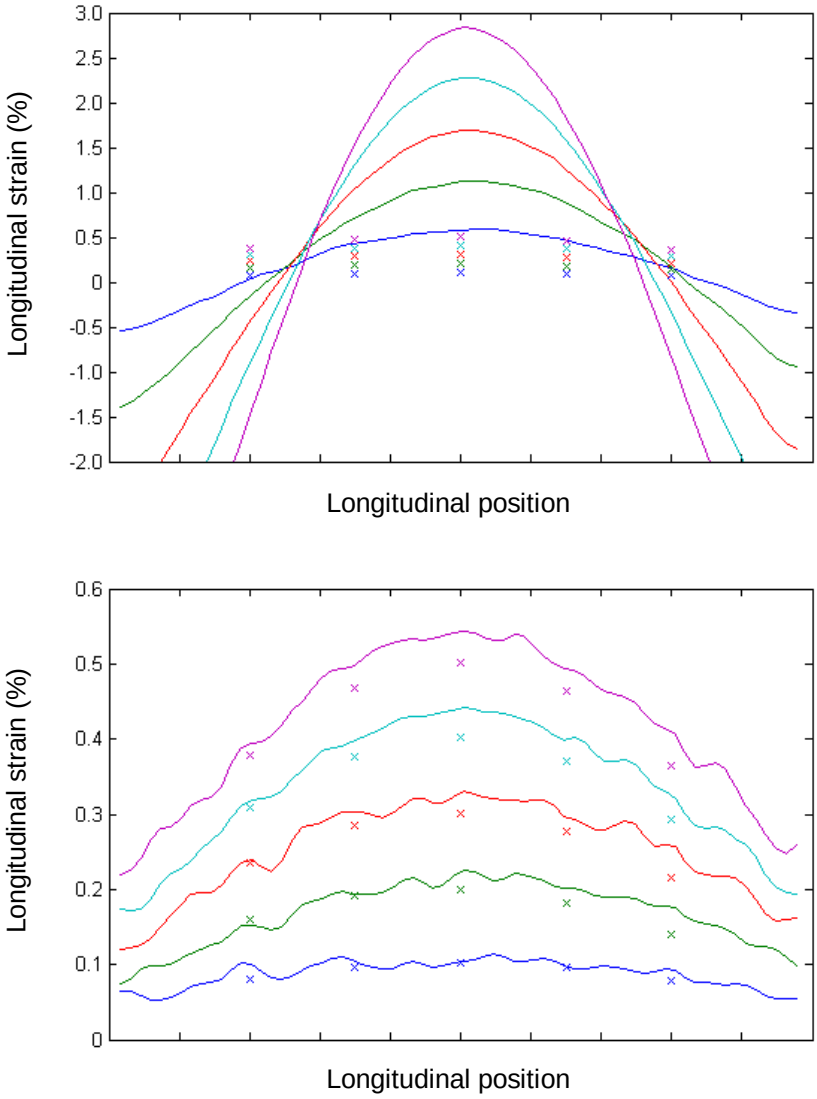

Figure 11: Resistance strain gauge measurements (points) vs. DIC measurements (lines) when performing a 2D analysis (top) vs. a 3D analysis (bottom)

While the observed out-of-plane displacement in this case was quite large, and was associated with correspondingly dramatic strain errors, experiments involving far more modest out-of-plane behaviour may also warrant the use 3D DIC. Figure 12 shows the errors associated with the use of 2D DIC for measuring the deformation of a polyurethane/steel sandwich composite specimen subjected to three-point bending. Out-of-plane displacement is defined to be in the z direction, with motion away from the camera corresponding to a positive z displacement.

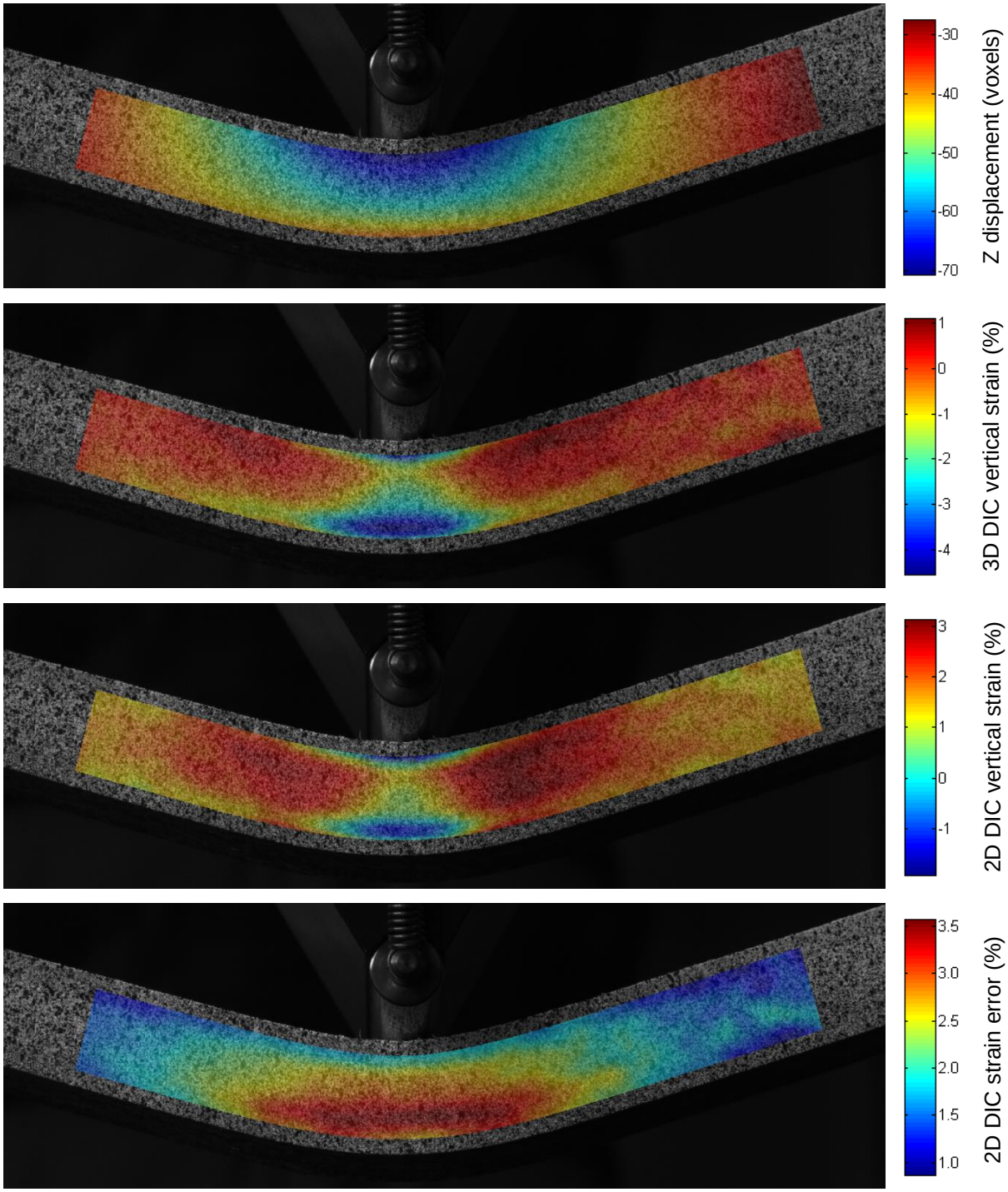

Figure 12: Axial strain error in a polyurethane/steel sandwich composite specimen subjected to three-point bending

Here it can be seen that, underneath the central loading pin and close to the tensile skin, the magnitude of the strain error was approximately the same as the real compressive deformation of the core that was measured using 3D DIC. The result of this was that the compressive deformation of the core was significantly underreported when using 2D DIC. There were two reasons for this large positive error. The first was that, since the camera was looking up at the specimen in order to ensure that the camera's view was not obscured by the loading pin, the specimen

was moving towards the camera as it deflected. The second was that, constrained by the skins, the surface of the core exhibited out-of-plane rotation as it bulged out towards the camera; this caused a positive error in the lower half of the core as it brought the surface's normal closer to the camera.

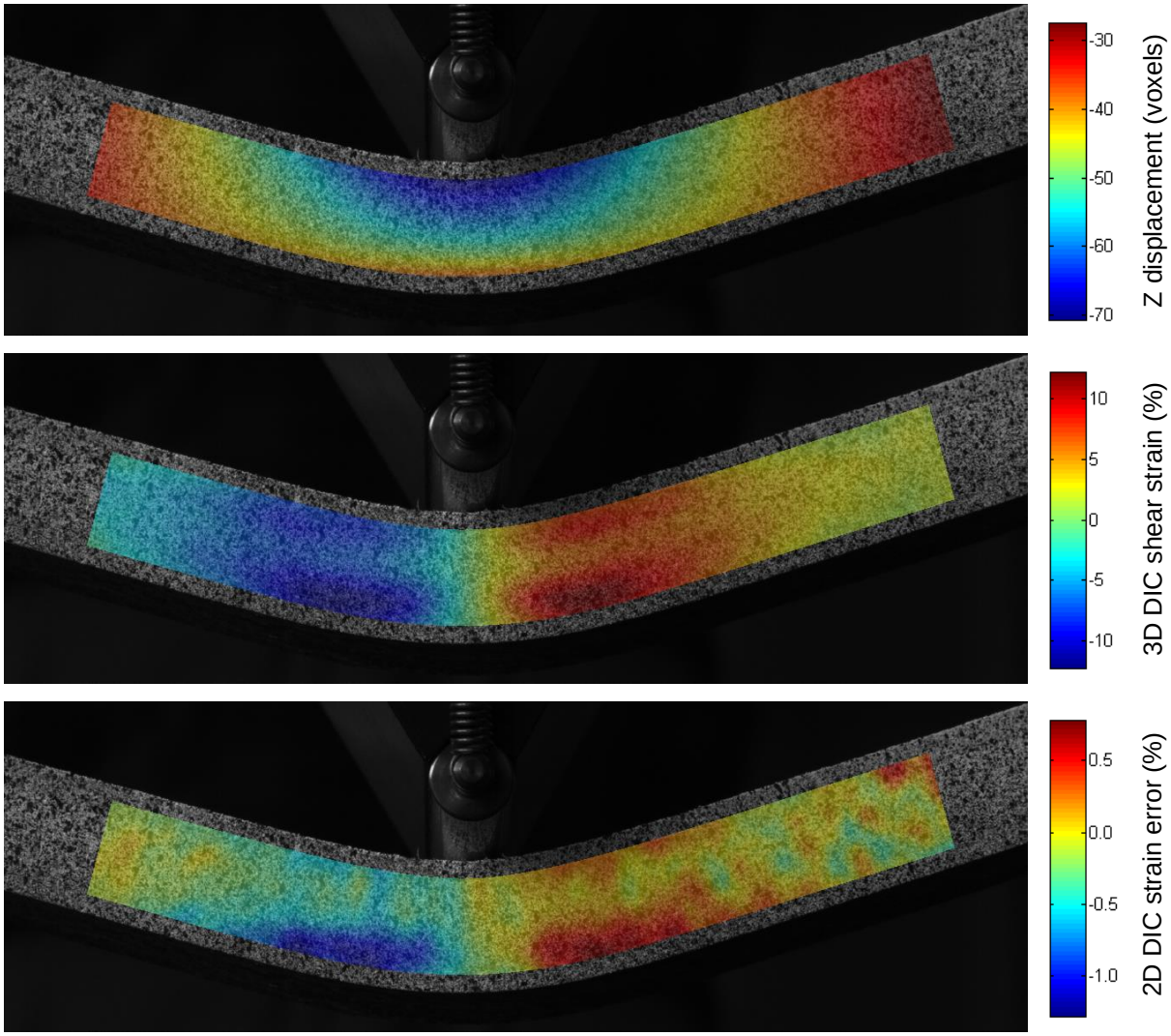

Figure 13: Shear strain error in a polyurethane/steel sandwich composite specimen subjected to three-point bending

The measurement errors related to the use of 2D DIC were less severe however when looking at the shear strains reported in the specimen, as shown in Figure 13. In this case the extent of the errors was an order of magnitude less than the strains measured in the core using 3D DIC. This is not unusual; the influence of out-of-plane displacements on shear strain measurements is small relative to their impact on axial strain measurements.

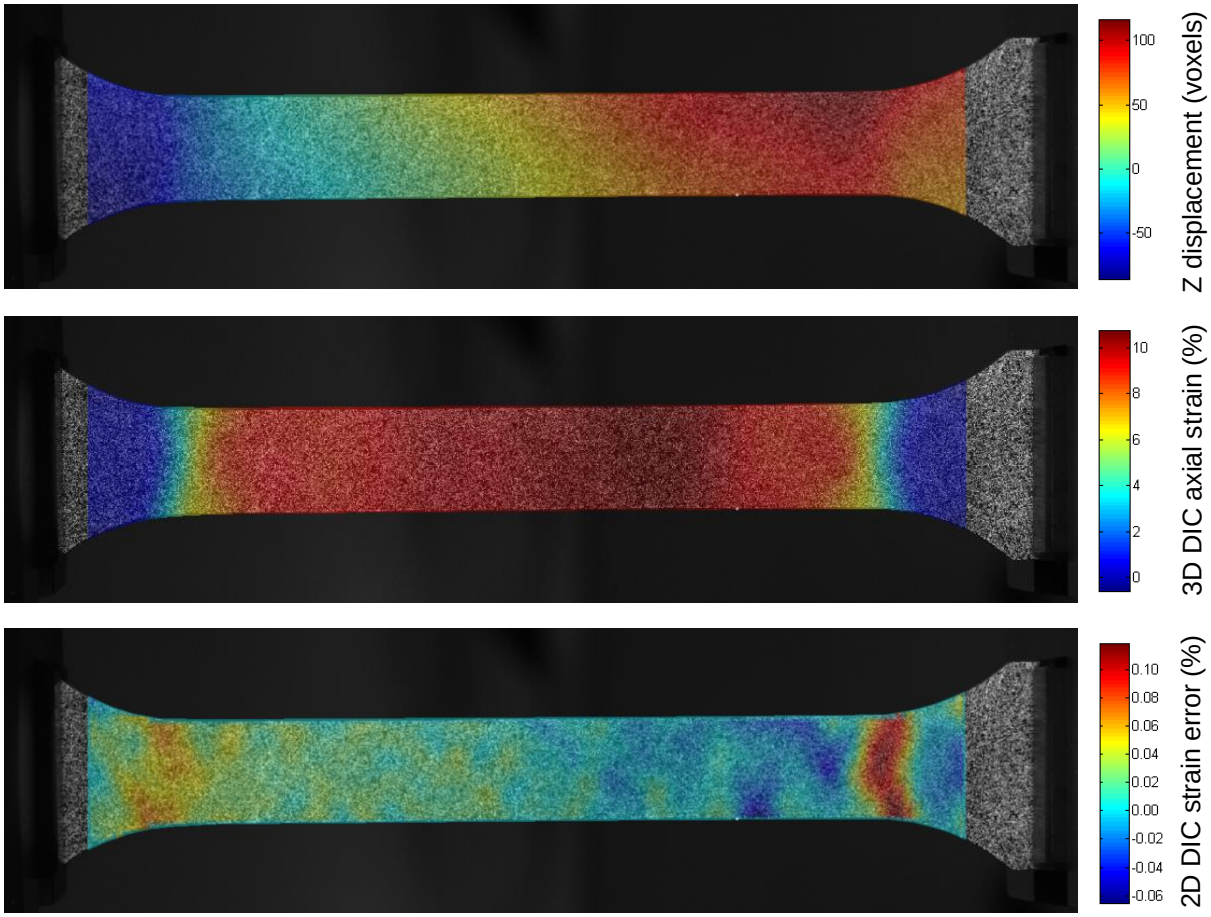

Figure 14: Strain error in an aluminium tensile specimen when using 2D DIC rather than 3D DIC

The measurement errors associated with the use of 2D DIC are quite small for experiments involving minimal out-of-plane displacements, such as the tensile test shown in Figure 14. In this case the maximum measurement error can be seen to be approximately two orders of magnitude smaller than the typical strain measured in the specimen. For experiments like this the causes of out-of-plane displacements tend to be: specimen bending or alignment during initial loading, contraction or expansion associated with the Poisson effect; and large in-plane displacements if the camera's optical axis is not quite normal to the surface. 3D DIC can be used for such experiments if desired, but in most cases the additional experimental complexity and computational cost associated with the use of 3D DIC is not justified.

3.3. Measurement precision

The measurement precision achievable when using Modεm is dependent on a wide range of factors including, but not limited to:

- Image noise
- Image spatial resolution
- Lens quality
- The quality of the surface's visual texture
- The presence of motion blur

- The selected tracking parameters
- The amount of smoothing applied
- The accuracy of any camera calibration that the user has performed

This wide array of variables, many of which are likely to be outside of the user's control, makes it difficult to identify a specific metric quantifying the system's accuracy. It is however possible to give an indication of the accuracy that a user might be able to expect of the system under typical conditions.

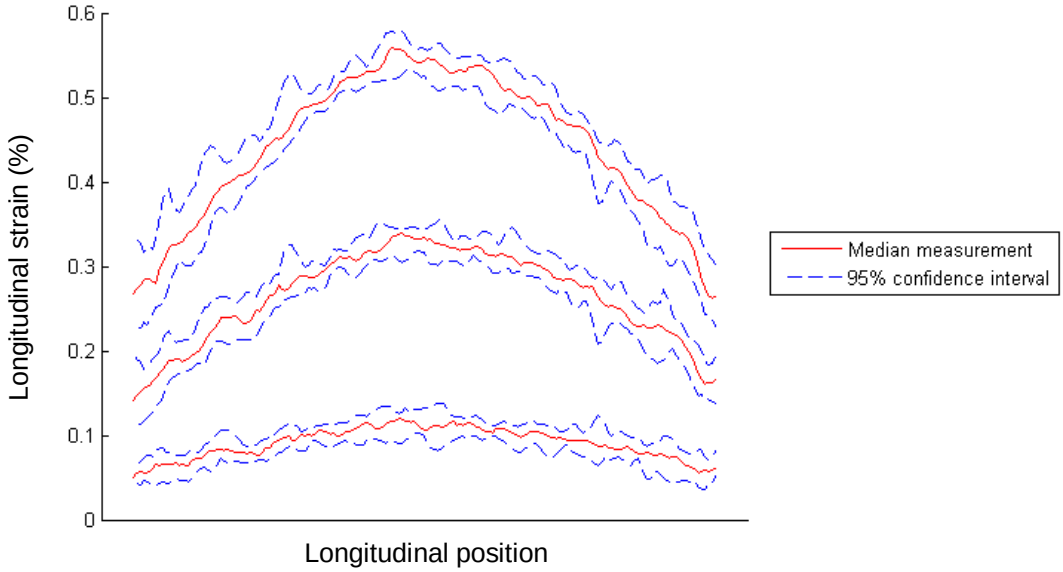

Figure 15: Indicative 3D DIC strain measurement variability at three different loads

Figure 15 shows the variability observed in the strains reported at three different deflections for the PVC buckling experiment described in section 3.2. This variability was observed by making repeated observations while varying the camera lenses, the stereo angle and the calibration pattern used. Multiple experiments were performed for each combination of these factors and multiple calibrations were repeated each time the lenses were changed or the cameras repositioned. The observed scatter also captures any real variability in the specimen's deformation for a given deflection.

For this experiment the typical observed standard deviation in the measured strains across all loads and longitudinal positions on the specimen was approximately 0.02%, or 200με, when a default amount of smoothing was applied. As mentioned earlier, many factors have an effect on the measurement precision achievable when using Modεm. These results are however considered to be indicative of the performance that might typically be expected when the system is employed effectively.

A conservative estimate of Modεm's performance is that, with the current hardware, a precision of 1000με or better can be achieved in most cases. Greater precision may be achievable in a number of instances, particularly for cases involving smooth

strain fields where significant smoothing can be applied to the measured displacements without detrimentally affecting the results.

4. CONCLUSIONS

DTA's AVS group now possesses a validated in-house DIC system, Modεm, that is capable of performing both 2D and 3D DIC-based analyses. A conservative estimate of Modεm's performance is that, with the current hardware, a precision of 1000με or better can be comfortably achieved in most cases. Greater precision may be achievable in a number of instances, particularly for cases involving smooth strain fields where significant smoothing can be applied to the measured displacements without detrimentally affecting the results.

This system is now available to enhance the AVS group's structural analysis toolset, providing a full-field strain measurement capability for New Zealand Defence Force platforms. In contrast to commercial DIC systems, this in-house system can be fully customised and adapted to suit individual New Zealand Defence Force requirements.

The flexibility of DIC as a technique for measuring both displacements and deformations results in a range of potential applications that is very broad. In general however, DIC is typically of the greatest value in applications where full-field results can provide intuitive insight into the behaviour of a structure or component, or where the use of conventional contact-based technologies such as resistance strain gauges is insufficient or overly burdensome.

REFERENCES

No Reference

[1] G. Vendroux and W. Knauss, “Submicron deformation field measurements: Part 2. Improved digital image correlation,” *Exp. Mech.*, vol. 38, no. 2, pp. 86–92, Jun. 1998.

[2] M. Ozbek, D. J. Rixen, O. Erne, and G. Sanow, “Feasibility of monitoring large wind turbines using photogrammetry,” *Energy*, vol. 35, no. 12, pp. 4802–4811, Dec. 2010.

[3] Correlated Solutions Inc, “VIC-3D System Specs,” *http://www.correlatedsolutions.com/index.php/products/vic-3d-2012/vic3d. Accessed: 04/12/2015*.

[4] B. P. Withy, “C1308: Summary of Steel Polyurethane Steel Sandwich Panel Testing,” Defence Technology Agency, 2015.

[5] S. Avril, M. Bonnet, A.-S. Bretelle, M. Grédiac, F. Hild, P. Ienny, F. Latourte, D. Lemosse, S. Pagano, E. Pagnacco, and F. Pierron, “Overview of Identification Methods of Mechanical Parameters Based on Full-field Measurements,” *Exp. Mech.*, vol. 48, no. 4, pp. 381–402, 2008.

[6] P. A. Hooper, R. A. M. Sukhram, B. R. K. Blackman, and J. P. Dear, “On the blast resistance of laminated glass,” *Int. J. Solids Struct.*, vol. 49, no. 6, pp. 899–918, Mar. 2012.

[7] V. Pickerd, “DSTO-TN-1203: Optimisation and Validation of the ARAMIS Digital Image Correlation System for use in Large-scale High-strain-rate Events,” Defence Science and Technology Organisation, 2013.

[8] T. Lundstrom, J. Baqersad, and C. Niezrecki, “Monitoring the Dynamics of a Helicopter Main Rotor With High-Speed Stereophotogrammetry,” *Exp. Tech.*, p. n/a–n/a, 2015.

[9] R. M. Stubbing and M. A. Battley, “Errors in Digital Image Correlation due to Colour Filter Array Interpolation,” in *Proceedings of ICEM 16*, 2014.

[10] J. Shi and C. Tomasi, “Good features to track,” in *Computer Vision and Pattern Recognition, 1994. Proceedings CVPR ’94., 1994 IEEE Computer Society Conference on*, 1994, pp. 593–600.

[11] R. M. Stubbing, “Characterisation of Polymeric Foam Cores Using Digital Image Correlation,” The University of Auckland, 2013.

[12] J. Bouguet, “Pyramidal implementation of the Lucas Kanade feature tracker,” *Intel Corp. Microprocess. Res. Labs*, 2000.

[13] S. Baker and I. Matthews, “Equivalence and efficiency of image alignment algorithms,” in *Computer Vision and Pattern Recognition, 2001. CVPR 2001.*

Proceedings of the 2001 IEEE Computer Society Conference on, 2001, vol. 1, pp. I–1090–I–1097 vol.1.

[14] M. A. Sutton, J.-J. Orteu, and H. W. Schreier, *Image correlation for shape, motion and deformation measurements*. Boston, MA: Springer US, 2009.

[15] B. Pan, “Reliability-guided digital image correlation for image deformation measurement.,” *Appl. Opt.*, vol. 48, no. 8, pp. 1535–1542, Mar. 2009.

[16] J. Heikkila and O. Silven, “A Four-step Camera Calibration Procedure with Implicit Image Correction,” in *Proceedings of the 1997 Conference on Computer Vision and Pattern Recognition (CVPR ’97)*, 1997, p. 1106–.

[17] Y. Gao, T. Cheng, Y. Su, X. Xu, Y. Zhang, and Q. Zhang, “High-efficiency and high-accuracy digital image correlation for three-dimensional measurement,” *Opt. Lasers Eng.*, vol. 65, pp. 73–80, Feb. 2015.

[18] R. Hartley and A. Zisserman, “Multiple view geometry in computer vision.” Cambridge University Press, Cambridge, UK; New York, 2003.

[19] M. A. Sutton, J. L. Turner, H. A. Bruck, and T. A. Chae, “Full-field representation of discretely sampled surface deformation for displacement and strain analysis,” *Exp. Mech.*, vol. 31, no. June, pp. 168–177, 1991.

[20] “MECH07/Aug15,” *AVS Group Technical Instuctions Manual*, vol. 2, Defence Technology Agency, 2015.

[21] “Cython - an overview,” *http://docs.cython.org/src/quickstart/overview.html. Accessed: 04/02/2016*.

[22] “ABOUT | OpenCV,” *http://opencv.org/about.html. Accessed: 04/02/2016*.

[23] S. Zike and L. P. Mikkelsen, “Correction of Gauge Factor for Strain Gauges Used in Polymer Composite Testing,” *Exp. Mech.*, vol. 54, no. 3, pp. 393–403, 2014.

APPENDIX A

DETERMINATION OF PARTIAL DERIVATIVES OF DISPLACEMENT WITH RESPECT TO Z

Deformation gradient:

$$F = \begin{bmatrix} \frac{\partial u}{\partial x} & \frac{\partial u}{\partial y} & \frac{\partial u}{\partial z} \\ \frac{\partial v}{\partial x} & \frac{\partial v}{\partial y} & \frac{\partial v}{\partial z} \\ \frac{\partial w}{\partial x} & \frac{\partial w}{\partial y} & \frac{\partial w}{\partial z} \end{bmatrix}$$

Right Cauchy-Green deformation tensor:

$$C = F^T F$$

Green-Lagrangian strain tensor:

$$E = \tfrac{1}{2}(C - I)$$

$$E = \begin{bmatrix} E_{xx} & E_{xy} & E_{xz} \\ E_{xy} & E_{yy} & E_{yz} \\ E_{xz} & E_{yz} & E_{zz} \end{bmatrix}$$

Enforcing a condition of plane-strain:

$$E_{xz} = E_{yz} = E_{zz} = 0$$

$$\Longrightarrow C_{13} = 0\,, C_{23} = 0\,, C_{33} = 1$$

Relating this back to the deformation gradient gives:

$$C_{13} = \left(1 + \frac{\partial u}{\partial x}\right)\frac{\partial u}{\partial z} + \frac{\partial v}{\partial x}\frac{\partial v}{\partial z} + \frac{\partial w}{\partial x}\left(1 + \frac{\partial w}{\partial z}\right) = 0$$

$$C_{23} = \frac{\partial u}{\partial y}\frac{\partial u}{\partial z} + \left(1 + \frac{\partial v}{\partial y}\right)\frac{\partial v}{\partial z} + \frac{\partial w}{\partial y}\left(1 + \frac{\partial w}{\partial z}\right) = 0$$

$$C_{33} = \left(\frac{\partial u}{\partial z}\right)^2 + \left(\frac{\partial v}{\partial z}\right)^2 + \left(\frac{\partial w}{\partial z}\right)^2 = 1$$

Solving for the three unknown partial derivatives then yields:

$$\frac{\partial u}{\partial z} = \frac{-\left(\frac{\partial w}{\partial x}\left(\frac{\partial v}{\partial y}+1\right)-\frac{\partial v}{\partial x}\frac{\partial w}{\partial y}\right)}{\sqrt{\begin{array}{c}\left(\frac{\partial u}{\partial x}+1\right)^2\left(\left(\frac{\partial v}{\partial y}+1\right)^2+\frac{\partial w}{\partial y}^2\right)-2\frac{\partial v}{\partial x}\left(\frac{\partial v}{\partial y}+1\right)\left(\left(\frac{\partial u}{\partial x}+1\right)\frac{\partial u}{\partial y}+\frac{\partial w}{\partial x}\frac{\partial w}{\partial y}\right)\\ -2\left(\frac{\partial u}{\partial x}+1\right)\frac{\partial w}{\partial x}\frac{\partial u}{\partial y}\frac{\partial w}{\partial y}+\left(\frac{\partial v}{\partial x}\right)^2\left(\left(\frac{\partial u}{\partial y}\right)^2+\left(\frac{\partial w}{\partial y}\right)^2\right)+\left(\frac{\partial w}{\partial x}\right)^2\left(\left(\frac{\partial u}{\partial y}\right)^2+\left(\frac{\partial v}{\partial y}+1\right)^2\right)\end{array}}}$$

$$\frac{\partial v}{\partial z} = \frac{-\left(\frac{\partial w}{\partial y}\left(\frac{\partial u}{\partial x}+1\right)-\frac{\partial u}{\partial y}\frac{\partial w}{\partial x}\right)}{\sqrt{\begin{array}{c}\left(\frac{\partial v}{\partial y}+1\right)^2\left(\left(\frac{\partial w}{\partial x}+1\right)^2+\frac{\partial w}{\partial x}^2\right)-2\frac{\partial v}{\partial y}\left(\frac{\partial u}{\partial x}+1\right)\left(\left(\frac{\partial v}{\partial y}+1\right)\frac{\partial v}{\partial x}+\frac{\partial w}{\partial y}\frac{\partial w}{\partial x}\right)\\ -2\left(\frac{\partial v}{\partial y}+1\right)\frac{\partial w}{\partial y}\frac{\partial v}{\partial x}\frac{\partial w}{\partial x}+\left(\frac{\partial u}{\partial y}\right)^2\left(\left(\frac{\partial v}{\partial x}\right)^2+\left(\frac{\partial w}{\partial x}\right)^2\right)+\left(\frac{\partial w}{\partial y}\right)^2\left(\left(\frac{\partial v}{\partial x}\right)^2+\left(\frac{\partial u}{\partial x}+1\right)^2\right)\end{array}}}$$

$$\frac{\partial w}{\partial z} = \sqrt{1-\left(\frac{\partial u}{\partial z}\right)^2-\left(\frac{\partial v}{\partial z}\right)^2}-1$$

DOCUMENT CONTROL SHEET

1.	ORIGINATING ACTIVITY Defence Technology Agency Auckland, New Zealand	2.	RELEASE AUTHORISED BY:
3.	REPORT NUMBER DTA Report 408	4.	CONTROL NUMBER NR 1690
5.	DATE February 2016	6.	NUMBER OF COPIES 8
7.	SECURITY CLASSIFICATION Unclassified	8.	RELEASE LIMITATIONS Nil
9.	TITLE DTA Digital Image Correlation Capability		
10.	AUTHOR(S) Richard M Stubbing	11.	AUTOMATIC DOWNGRADING
12.	KEYWORDS Digital image correlation, full-field strain measurement, photogrammetry		

13. ABSTRACT

Digital Image Correlation (DIC) is a technique for optically acquiring full-field measurements of the displacement and deformation of a surface. This is achieved by observing the surface as it deforms, typically using one or more conventional monochrome digital cameras, and comparing the surface's deformed and undeformed states using optical tracking.

The Defence Technology Agency's Applied Vehicle Systems group has now developed an in-house DIC system. The wide array of variables that determine the measurement precision achievable when using DIC makes it difficult to identify a specific metric quantifying this system's accuracy. However, a conservative estimate is that deformation measurements can be obtained with a precision of 1000 microstrain or better in most cases. Greater precision may be achievable in a number of instances, particularly for cases involving smooth strain fields where significant smoothing can be applied to the measured displacements without detrimentally affecting the results.

This system is now available to enhance the Applied Vehicle Systems group's structural analysis toolset, providing a full-field strain measurement capability for New Zealand Defence Force platforms. In contrast to commercial DIC systems, this in-house system can be fully customised and adapted to suit individual New Zealand Defence Force requirements.

New Zealand
DEFENCE
FORCE
Te Ope Kātua O Aotearoa

DEFENCE TECHNOLOGY AGENCY

Devonport Naval Base.
Private Bag 32901.
Devonport, Auckland
New Zealand 0744

T +64 (0)9 445 5902
F +64 (0)9 445 5890
www.dta.mil.nz